Expert Systems with Applications 39 (2012) 4710–4717

Contents lists available at SciVerse ScienceDirect

Expert Systems with Applications

journal homepage: www.elsevier.com/locate/eswa

Evolutionary RBF classifier for polarimetric SAR images

Turker Ince [a,*], Serkan Kiranyaz [b], Moncef Gabbouj [b]

[a] Izmir University of Economics, Electronics and Telecommunications Engineering Department, Izmir, Turkey
[b] Tampere University of Technology, Department of Signal Processing, Tampere, Finland

ARTICLE INFO

Keywords:
Polarimetric synthetic aperture radar
Radial basis function network
Particle swarm optimization

ABSTRACT

In this paper, a robust radial basis function (RBF) network based classifier is proposed for polarimetric synthetic aperture radar (SAR) images. The proposed feature extraction process utilizes the covariance matrix elements, the H/α/A decomposition based features combined with the backscattering power (span), and the gray level co-occurrence matrix (GLCM) based texture features, which are projected onto a lower dimensional feature space using principal components analysis. For the classifier training, both conventional backpropagation (BP) and multidimensional particle swarm optimization (MD-PSO) based dynamic clustering are explored. By combining complete polarimetric covariance matrix and eigenvalue decomposition based pixel values with textural information (contrast, correlation, energy, and homogeneity) in the feature set, and employing automated evolutionary RBF classifier for the pattern recognition unit, the overall classification performance is shown to be significantly improved. An experimental study is performed using the fully polarimetric San Francisco Bay and Flevoland data sets acquired by the NASA/Jet Propulsion Laboratory Airborne SAR (AIRSAR) at L-band to evaluate the performance of the proposed classifier. Classification results (in terms of confusion matrix, overall accuracy and classification map) compared with the major state of the art algorithms demonstrate the effectiveness of the proposed RBF network classifier.

1. Introduction

Image and data classification techniques play an important role in the automatic analysis and interpretation of remote sensing data. Particularly polarimetric synthetic aperture radar (SAR) data poses a challenging problem in this field due to complexity of measured information from its multiple polarimetric channels. Recently, the number of applications which use data provided by the SAR systems having fully polarimetric capability have been increasing. Over the past decade, there has been extensive research in the area of the segmentation and classification of polarimetric SAR data. In the literature, the classification algorithms for polarimetric SAR can be divided into three main classes: (1) classification based on physical scattering mechanisms inherent in data (Pottier & Lee, 2000; van Zyl, 1989), (2) classification based on statistical characteristics of data (Lee et al., 1999; Wu, Ji, Yu, & Su, 2008) and (3) classification based on image processing techniques (Ince, 2010; Tan, Lim, & Ewe, 2007; Ye & Lu, 2002). Additionally, there has been several works using some combinations of the above classification approaches (Lee et al., 1999; Pottier & Lee, 2000). While these approaches to the polarimetric SAR classification problem can be based on either supervised or unsupervised methods, their performance and suitability usually depend on applications and the availability of ground truth.

As one of the earlier algorithms, Kong, Swartz, Yueh, Novak, and Shin (1988) derived a distance measure based on the complex Gaussian distribution and used it for maximum-likelihood (ML) classification of single-look complex polarimetric SAR data. Then, Lee, Grunes, and Kwok (1994) used the statistical properties of a fully polarimetric SAR to perform a supervised classification based on complex Wishart distribution. Afterwards, Cloude and Pottier (1997) proposed an unsupervised classification algorithm based on their target decomposition theory. Target entropy (H) and target average scattering mechanism (scattering angle, α) calculated from this decomposition have been widely used in polarimetric SAR classification. For multilook data represented in covariance or coherency matrices, Lee et al. (1999) proposed a new unsupervised classification method based on combination of polarimetric target decomposition (Cloude & Pottier, 1997) and the maximum likelihood classifier using the complex Wishart distribution. The unsupervised Wishart classifier has an iterative procedure based on the well-known *K-means* algorithm, and has become a preferred benchmark algorithm due to its computational efficiency and generally good performance. However, this classifier still has some significant drawbacks since it entirely relies on *K-means* for actual clustering, such as it may converge to local optima, the number of clusters should be fixed *a priori*, its performance is sensitive to the

* Corresponding author. Tel.: +90 2324888509; fax: +90 2324888475.
E-mail address: turker.ince@ieu.edu.tr (T. Ince).

0957-4174/$ - see front matter © 2011 Elsevier Ltd. All rights reserved.
doi:10.1016/j.eswa.2011.09.082

initialization and its convergence depends on several parameters. Recently, a two-stage unsupervised clustering based on the EM algorithm (Khan, Yang, & Zhang, 2007) is presented for classification of polarimetric SAR images. The EM algorithm estimates parameters of the probability distribution functions which represent the elements of a 9-dimensional feature vector, consisting of six magnitudes and three angles of a coherency matrix. Markov random field (MRF) clustering based method (Tran, Wehrens, Hoekman, & Buydens, 2005) exploiting the spatial relation between adjacent pixels in polarimetric SAR images has been presented. In (Ye & Lu, 2002), a new wavelet-based texture image segmentation algorithm is successfully applied to unsupervised SAR image segmentation problem.

More recently, neural network based approaches (Yang, Wang, & Jiao, 2009; Zhang, Wu, & Wei, 2009; Zhang, Zou, Zhang, & Zhang, 2010) for classification of polarimetric synthetic aperture radar data have been shown to outperform other aforementioned well-known techniques. Compared with other approaches, neural network classifiers have the advantage of adaptability to the data without making *a priori* assumption of a particular probability model or distribution. However, their performance depends on the network structure, training data, initialization, and parameters. Designing an optimal ANN classifier structure and its parameters to maximize the classification accuracy is still a crucial and challenging task. In this study, RBF network classifier which is optimally designed by the evolutionary search technique, multidimensional particle swarm optimization (MD-PSO) (Kiranyaz, Ince, Yildirim, & Gabbouj, 2010), is employed. RBFs are chosen due to their robustness, faster learning capability compared with other feedforward networks, and superior performance with simpler network architectures. Earlier work on RBF classifiers for polarimetric SAR image classification has demonstrated a potential for performance improvement over conventional techniques (Ince, 2010). The proposed polarimetric SAR feature vector includes full covariance matrix, the H/α/A decomposition based features combined with the backscattering power (*Span*), and the gray level co-occurrence matrix (GLCM) based texture features as suggested by the results of previous studies (Clausi & Yue, 2004; Ersahin, Scheuchl, & Cumming, 2004). The performance of the proposed RBF network based classifier is evaluated using the fully polarimetric San Francisco Bay and Flevoland data sets acquired by the NASA/Jet Propulsion Laboratory Airborne SAR (AIRSAR) at L-band. The classification results (in terms of confusion matrix, overall accuracy and classification map) are compared with competing state of the art classifiers.

The rest of the paper is organized as follows. Section 2 briefly presents the basic theory of polarimetric SAR for this paper including the Cloude–Pottier decomposition. The feature extraction methodology for the proposed polarimetric SAR image classification system is described in Section 3. Then, the RBF network fundamentals, its training algorithms, and an overview of the proposed classifier technique are presented in Section 4. Section 5 describes the experimental test results on real polarimetric SAR data. Finally, Section 6 concludes the paper.

2. Polarimetric sar data processing

Polarimetric radars often measure the complex scattering matrix, $[S]$, produced by a target under study with the objective to infer its physical properties. Assuming linear horizontal and vertical polarizations for transmitting and receiving, $[S]$ can be expressed as

$$S = \begin{bmatrix} S_{hh} & S_{hv} \\ S_{vh} & S_{vv} \end{bmatrix} \tag{1}$$

Reciprocity theorem applies in a monostatic system configuration, $S_{hv} = S_{vh}$. For coherent scatterers only, the decompositions of the measured scattering matrix $[S]$ can be employed to characterize the scattering mechanisms of such targets. One way to analyze coherent targets is the Pauli decomposition (Lee et al., 1999), which expresses $[S]$ in the so-called Pauli basis $\left\{ [S]_a = \frac{1}{\sqrt{2}} \begin{bmatrix} 1 & 0 \\ 0 & 1 \end{bmatrix}, \right.$ $[S]_b = \frac{1}{\sqrt{2}} \begin{bmatrix} 1 & 0 \\ 0 & -1 \end{bmatrix}$, $\left. [S]_c = \frac{1}{\sqrt{2}} \begin{bmatrix} 0 & 1 \\ 1 & 0 \end{bmatrix} \right\}$ as,

$$S = \begin{bmatrix} S_{hh} & S_{hv} \\ S_{vh} & S_{vv} \end{bmatrix} = \alpha[S]_a + \beta[S]_b + \gamma[S]_c \tag{2}$$

where $\alpha = (S_{hh} + S_{vv})/\sqrt{2}, \beta = (S_{hh} - S_{vv})/\sqrt{2}, \gamma = \sqrt{2}S_{hv}$. Hence, by means of the Pauli decomposition, all polarimetric information in $[S]$ could be represented in a single RGB image by combining the intensities $|\alpha|^2, |\beta|^2$ and $|\gamma|^2$, which determine the power scattered by different types of scatterers such as single- or odd-bounce scattering, double- or even-bounce scattering, and orthogonal polarization returns by the volume scattering. There are several other coherent decomposition theorems such as the Krogager decomposition, the Cameron decomposition, and SDH (Sphere, Diplane, Helix) decomposition all of which aim to express the measured scattering matrix by the radar as the combination of scattering responses of coherent scatterers.

Alternatively, the second order polarimetric descriptors of the average polarimetric covariance $\langle[C]\rangle$ and the coherency $\langle[T]\rangle$ matrices can be derived from the scattering matrix and employed to extract physical information from the observed scattering process. The elements of the covariance matrix, $[C]$, can be written in terms of three unique polarimetric components of complex scattering matrix:

$$\begin{aligned} C_{11} &= S_{hh}S_{hh}^*, \quad C_{21} = S_{hh}^*S_{hv} \\ C_{22} &= S_{hv}S_{hv}^*, \quad C_{32} = S_{hh}^*S_{vv} \\ C_{33} &= S_{vv}S_{vv}^*, \quad C_{11} = S_{hh}^*S_{vv} \end{aligned} \tag{3}$$

For single-look processed polarimetric SAR data, the three polarimetric components (*HH*, *HV*, and *VV*) has a multivariate complex Gaussian distribution and the complex covariance matrix form has a complex Wishart distribution (Lee et al., 1994). Due to presence of speckle noise and random vector scattering from surface or volume, polarimetric SAR data are often multi-look processed by averaging n neighboring pixels. By using the Pauli based scattering matrix for a pixel i, $k_i = [S_{hh} + S_{vv}, S_{hh} - S_{vv}, 2S_{hv}]^T/\sqrt{2}$, the multi-look coherency matrix, $\langle[T]\rangle$, can be written as

$$\langle T \rangle = \frac{1}{n}\sum_{i=1}^{n} k_i k_i^{*T} \tag{4}$$

Both coherency $\langle[T]\rangle$ and covariance $\langle[C]\rangle$ are 3×3 Hermitian positive semidefinite matrices, and since they can be converted into one another by a linear transform, both are equivalent representations of the target polarimetric information.

The incoherent target decomposition theorems such as the Freeman decomposition, the Huynen decomposition, and the Cloude–Pottier (or H/α/A) decomposition employ the second order polarimetric representations of PolSAR data (such as covariance matrix or coherency matrix) to characterize distributed scatterers. The H/α/A decomposition (Cloude & Pottier, 1996) is based on eigen analysis of the polarimetric coherency matrix, $\langle[T]\rangle$:

$$\langle T \rangle = \lambda_1 e_1 e_1^{*T} + \lambda_2 e_2 e_2^{*T} + \lambda_3 e_3 e_3^{*T} \tag{5}$$

where $\lambda_1 > \lambda_2 > \lambda_3 \geqslant 0$ are real eigenvalues and the corresponding orthonormal eigenvectors e_i (representing three scattering mechanisms) are

$$e_i = e^{i\phi_i}[\cos\alpha_i, \sin\alpha_i \cos\beta_i e^{i\delta_i}, \sin\alpha_i \sin\beta_i e^{i\gamma_i}]^T \tag{6}$$

Cloude and Pottier defined entropy H, average of set of four angles $\bar{\alpha}$, $\bar{\beta}$, $\bar{\delta}$, and $\bar{\gamma}$, and anisotropy A for analysis of the physical information related to the scattering characteristics of a medium:

$$H = -\sum_{i=1}^{3} p_i \log_3 p_i \quad \text{where} \quad p_i = \frac{\lambda_i}{\sum_{i=1}^{3}\lambda_i} \tag{7}$$

$$\bar{\alpha} = \sum_{i=1}^{3} p_i\alpha_i, \;\; \bar{\beta} = \sum_{i=1}^{3} p_i\beta_i, \;\; \bar{\delta} = \sum_{i=1}^{3} p_i\delta_i, \;\; \bar{\gamma} = \sum_{i=1}^{3} p_i\gamma_i \tag{8}$$

$$A = \frac{p_2 - p_3}{p_2 + p_3} \tag{9}$$

For a multi-look coherency matrix, the entropy, $0 \leqslant H \leqslant 1$, represents the randomness of a scattering medium between isotropic scattering ($H = 0$) and fully random scattering ($H = 1$), while the average alpha angle can be related to target average scattering mechanisms from single-bounce (or surface) scattering ($\bar{\alpha} \approx 0$) to dipole (or volume) scattering ($\bar{\alpha} \approx \pi/4$) to double-bounce scattering ($\bar{\alpha} \approx \pi/2$). Due to basis invariance of the target decomposition, H and $\bar{\alpha}$ are roll invariant hence they do not depend on orientation of target about the radar line of sight. Additionally, information about target's total backscattered power can be determined by the *span* as

$$span = \sum_{i=1}^{3} \lambda_i \tag{10}$$

Entropy (H), estimate of the average alpha angle ($\bar{\alpha}$), and *span* calculated by the above noncoherent target decomposition method have been commonly used as polarimetric features of a scatterer in many target classification schemes (Fang, Wen, & Yirong, 2006; Lee et al., 1999).

3. Feature extraction

The proposed feature extraction process utilizes the complete covariance matrix information, the gray level co-occurrence matrix (GLCM) based texture features, and the backscattering power (*span*) combined with the $H/\alpha/A$ decomposition (Cloude & Pottier, 1997). The feature vector from the Cloude–Pottier decomposition includes entropy (H), anisotropy (A), estimates of the set of average angles ($\bar{\alpha}$, $\bar{\beta}$, $\bar{\delta}$, and $\bar{\gamma}$), three real eigenvalues ($\lambda_1, \lambda_2, \lambda_3$), and *span*. As suggested by the previous studies (Clausi, 2002; Zhang et al., 2009) appropriate texture measures for SAR imagery based on the gray level co-occurrence probabilities are included in the feature set to improve its discrimination power and classification accuracy. In this study, *contrast*, *correlation*, *energy*, and *homogeneity* features are extracted from normalized GLCMs which are calculated using interpixel distance of 2 and averaging over four possible orientation settings ($\theta = 0°, 45°, 90°, 135°$). To reduce the dimensionality (and redundancy) of input feature space, the principal components transform is applied to these inputs and the most principal components (which contain about 95% of overall energy in the original feature matrix) are then selected to form a resultant feature vector for each imaged pixel. Dimensionality reduction of input feature information improves efficiency of learning for a neural network classifier due to a smaller number of input nodes (to avoid curse of dimensionality) (Pittner & Kamarthi, 1999) and reduces computation time. For the purpose of normalizing and scaling the feature vector, each feature dimension is first normalized to have a zero mean and unity standard deviation before principal component analysis (PCA) is applied, and following the PCA outputs are linearly scaled into $[-1, 1]$ interval.

4. RBF neural networks

An artificial neural network (ANN) consists of a set of connected processing units, usually called neurons or nodes. ANNs can be described as directed graphs, where each node performs some activation function to its inputs and then gives the result forward to be the input of some other neurons until the output neurons are reached. ANNs can be divided into feedforward and recurrent networks according to their connectivity. In a recurrent ANN there can be backward loops in the network structure, while in feedforward ANNs such loops are not allowed. A popular type of feedforward ANN is the radial basis function (RBF) network (Poggio & Girosi, 1989), which has always two layers in addition to the passive input layer: a hidden layer of RBF units and a linear output layer. Only the output layer has connection weights and biases. The activation function of the kth RBF unit is defined as

$$y_k = \varphi\left(\frac{\|X - \mu_k\|}{\sigma_k^2}\right) \tag{11}$$

where φ is a radial basis function or, in other words, a strictly positive radially symmetric function, which has a unique maximum at N-dimensional center μ_k and whose value drops rapidly close to zero away from the center. σ_k is the width of the peak around the center μ_k. The activation function gets noteworthy values only when the distance between the N-dimensional input X and the center μ_k, $\|X - \mu_k\|$ is smaller than the width σ_k. The most commonly used activation function in RBF networks is the Gaussian basis function defined as

$$y_k = \exp\left(-\frac{\|X - \mu_k\|^2}{2\sigma_k^2}\right) \tag{12}$$

where μ_k and σ_k are the mean and standard deviation, respectively, and $\|\cdot\|$ denotes the Euclidean norm. More detailed information about RBF networks can be obtained from Poggio and Girosi (1989) and Haykin (1998).

In this study, two distinct training methods for RBF network classifiers, the traditional backpropagation (BP) and particle swarm optimization (PSO) are investigated. For the BP algorithm, RPROP enhancement is used when training RBF networks. The main difference in RPROP is that it modifies the update-values for each parameter according to the sequence of signs of partial derivatives. This only leads to a faster convergence, while the problems of a hill-climbing algorithm are not solved. Further details about BP and RPROP can be found in Chauvin and Rumelhart (1995) and Riedmiller and Braun (1993), respectively. In order to determine (near-) optimal network architecture for a given problem, we apply exhaustive BP training over every network configuration in the architecture space defined. For PSO-based training, the proposed approach is to apply multi-dimensional particle swarm optimization (MD-PSO) based dynamic clustering (Kiranyaz, Ince, Yildirim, & Gabbouj, 2009) to determine the optimal (with respect to minimizing a given cost function for the input–output mapping) number of Gaussian neurons with their correct parameters (centroids and variances). Afterwards, BP can conveniently be used to compute the remaining network parameters, weights (w) and bias (θ) of the each output layer neuron. The overview of the proposed classifier for polarimetric SAR image is shown in Fig. 1.

5. Experimental results

In this section, two test images of an urban area (San Francisco Bay, CA) and an agricultural area (Flevoland in the Netherlands), both acquired by the NASA/Jet Propulsion Laboratory's Airborne SAR (AIRSAR) at L-band, were chosen for performance evaluation of the proposed RBF network classifier. Both data sets

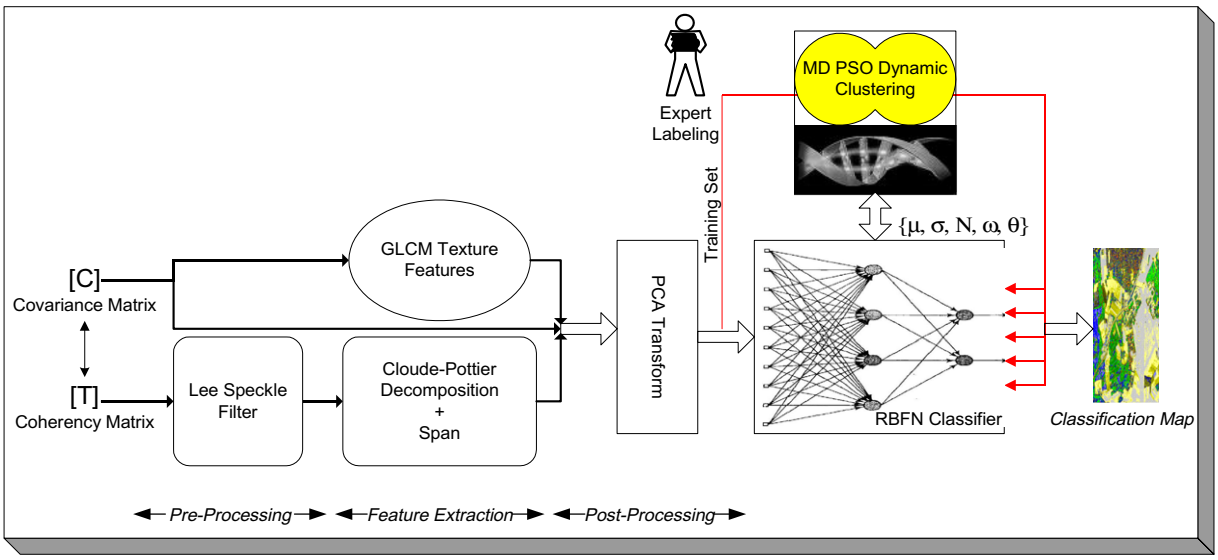

Fig. 1. Overview of the evolutionary RBF network classifier design for polarimetric SAR image.

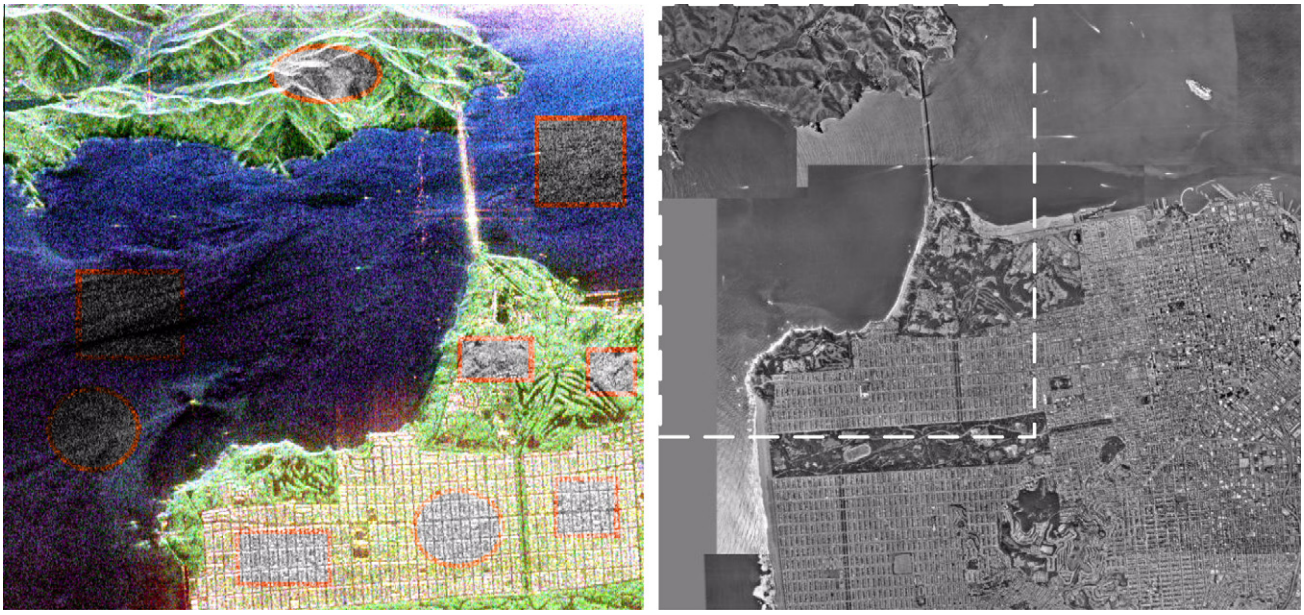

Fig. 2. Pauli image of 600 × 600 pixel sub-area of San Francisco Bay (left) with the 5 × 5 refined Lee filter used. The training and testing areas for three classes are shown using red rectangles and circles respectively. The aerial photograph for this area (right) provided by the US Geological Survey taken on October, 1993 can be used as ground-truth. (For interpretation of the references to color in this figure legend, the reader is referred to the web version of this article.)

have been widely used in the polarimetric SAR literature over the last two decades (Ersahin et al., 2004; Ferro-Famil, Pottier, & Lee, 2001; Fukuda & Hirosawa, 1999), and distributed as multi-look processed and publicly available through the polarimetric SAR data processing and educational tool (PolSARpro) by ESA (The Polarimetric SAR Data Processing and Educational Tool (PolSARPro). The original four-look fully polarimetric SAR data of the San Francisco Bay, having a dimension of 900 × 1024 pixels, provides good coverage of both natural (sea, mountains, forests, etc.) and man-made targets (buildings, streets, parks, golf course, etc.) with a more complex inner structure. For the purpose of comparing the classification results with the Wishart (Lee et al., 1999) and the NN-based (Zhang et al., 2009) classifiers, the sub-area (Fig. 2) with size 600 × 600 is extracted and used. The aerial photographs for this area which can be used as ground-truth are provided by the TerraServer Web site (U.S. Geological Survey Images). In this study, no speckle filtering is applied to originally four-look processed covariance matrix data and before GLCM based texture feature generation to retain the resolution and to preserve the texture information. However, additional averaging, such as using the polarimetry preserving refined Lee filter (Lee, Grunes, & de Grandi, 1999) with 5 × 5 window, of coherency matrix should be performed prior to the Cloude–Pottier decomposition (Cloude & Pottier, 1997). For MD-PSO based clustering algorithm, the typical internal PSO parameters (c_1, c_2 and w) are used as in Shi and Eberhart (1998), also explained in Kiranyaz, Ince, Yildirim, and Gabbouj (2009). For all experiments in this section, the two critical PSO parameters, swarm size (S) and number of iterations ($IterNo$), are set as 40 and 1000, respectively.

To test the performance of the proposed classifier and compare its classification results, the same training and testing areas for the three classes from the sub San Francisco area (as shown on the Pauli-based decomposition image in Fig. 2), the sea (15,810, 6723 pixels respectively), urban areas (9362, 6800), and the vegetated zones (5064, 6534), which are manually selected in an earlier study (Zhang et al., 2009), are used. The confusion matrix of the proposed evolutionary RBF method on the training and testing areas are given in Table 1. The classification accuracy values are averaged over 10 independent runs. From the results, the main drawback of the proposed method is the separation of vegetated zones from urban areas. Compared to two other competing techniques, the proposed method is able to differentiate better the uniform areas corresponding to main classes of scattering such asthe ocean, vegetation, and building areas. In Table 2, the overall accuracies in training and testing areas for the proposed RBF classifier trained using the BP and MD-PSO algorithms and two competing methods, the Wishart Maximum Likelihood (WML) classifier (Lee et al., 1999) and the NN-based classifier (Zhang et al., 2009), are compared. The average accuracies over 10 independent runs for the best configuration of the RBF-BP and RBF-PSO classifiers are reported. The proposed RBF classifier trained by the global PSO algorithm is superior to the NN-based, WML, and RBF-BP based methods with higher accuracies in both training (99.50%) and testing (98.96%) areas. Fig. 3 shows the classification results on the whole sub-area image for the RBF-PSO based classifier. The classification map of the whole San Francisco Bay image produced by the same classifier is given in Fig. 4 for a qualitative (visual) performance evaluation. The evolutionary RBF classifier has the structure of 11 input neurons, 21 Gaussian neurons which the cluster centroids and variance (μ_k and σ_k) are determined by MD-PSO based dynamic clustering the training data, and 3 output neurons.

The classification results in Table 2 have been produced by using a high percentage (60%) of total (training and testing combined) pixels for training. The proposed classifier is also tested by limiting the percentage of total pixels which were used for classifier training to less than 1% of the total pixels to be classified. The results over the same testing data set are shown in Table 3. In this case, the RBF network classifier trained by the BP or MD-PSO algorithms performed still at a high level, achieving accuracies over 95% and 98% respectively. Generally, a relatively smaller training data set can avoid over-fitting and improve generalization performance of a classifier over larger data sets.

In order to test robustness of the proposed RBF network classifier trained by the MD-PSO based dynamic clustering, 20 independent runs are performed over the San Francisco area image and the resulting cluster number histogram is plotted in Fig. 5. Additionally, the plots of a typical run showing the fitness score and dimension versus number of iterations for MD-PSO operation are presented in the left side of Fig. 5. Based on overall clustering results, it is found that the number of clusters (the optimal number of Gaussian neurons) and their centroids extracted from the MD-PSO based dynamic clustering are generally consistent, indicating the proposed technique is robust (or repeatable).

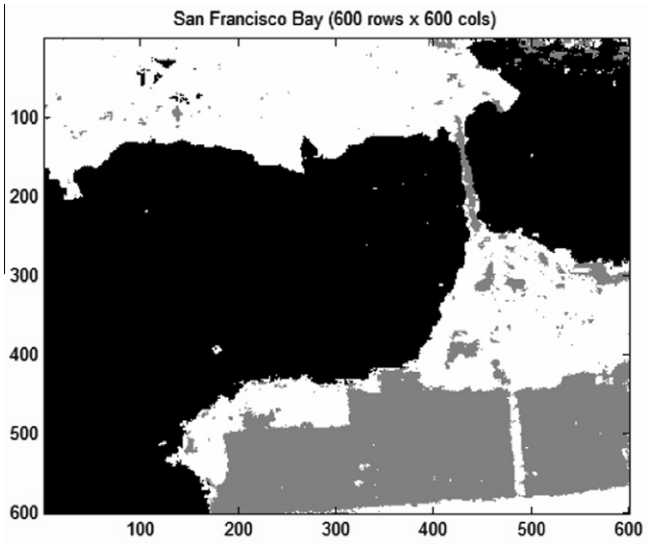

Fig. 3. The classification results of the proposed RBF-PSO technique on the extracted 600 × 600 sub-image of San Francisco Bay (black denotes sea, gray urban areas, white vegetated zones).

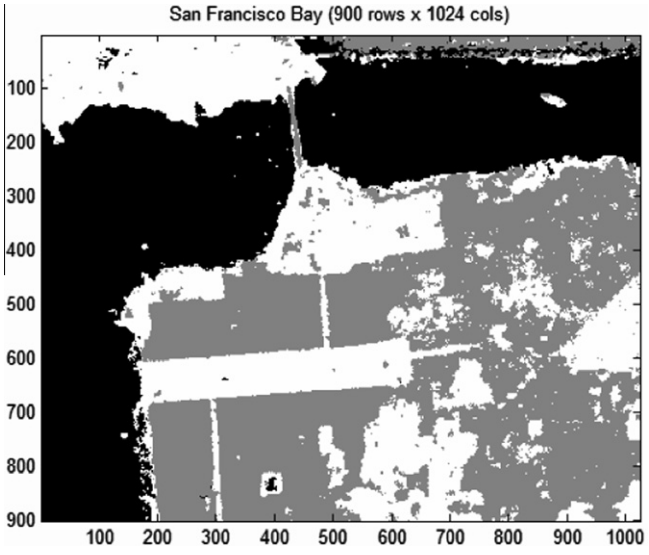

Fig. 4. The classification results of the proposed RBF-MDPSO technique for the original (900 × 1024) San Francisco Bay image (black denotes sea, gray urban areas, white vegetated zones).

Table 1
Summary table of pixel-by-pixel classification results of the proposed RBF-MDPSO method for the training and testing data of San Francisco Bay.

	Training data			Test data		
	Sea	Urb	Veg	Sea	Urb	Veg
Sea	14,264	4	0	6804	0	0
Urb	11	9422	22	10	6927	23
Veg	10	87	4496	21	162	6786

Table 2
Overall performance comparison (in percent) for San Francisco Bay dataset. The best performances are indicated in bold.

Method	Training area	Testing area
RBF-BP	98.00	95.70
WML (Lee et al., 1999)	97.23	96.16
NN (Zhang et al., 2009)	99.42	98.64
RBF-PSO	**99.50**	**98.96**

Table 3
Overall performance (in percent) using smaller training set (<1% of total pixels) for San Francisco Bay dataset.

Method	Training area	Testing area
RBF-BP	100	95.60
RBF-PSO	100	98.54

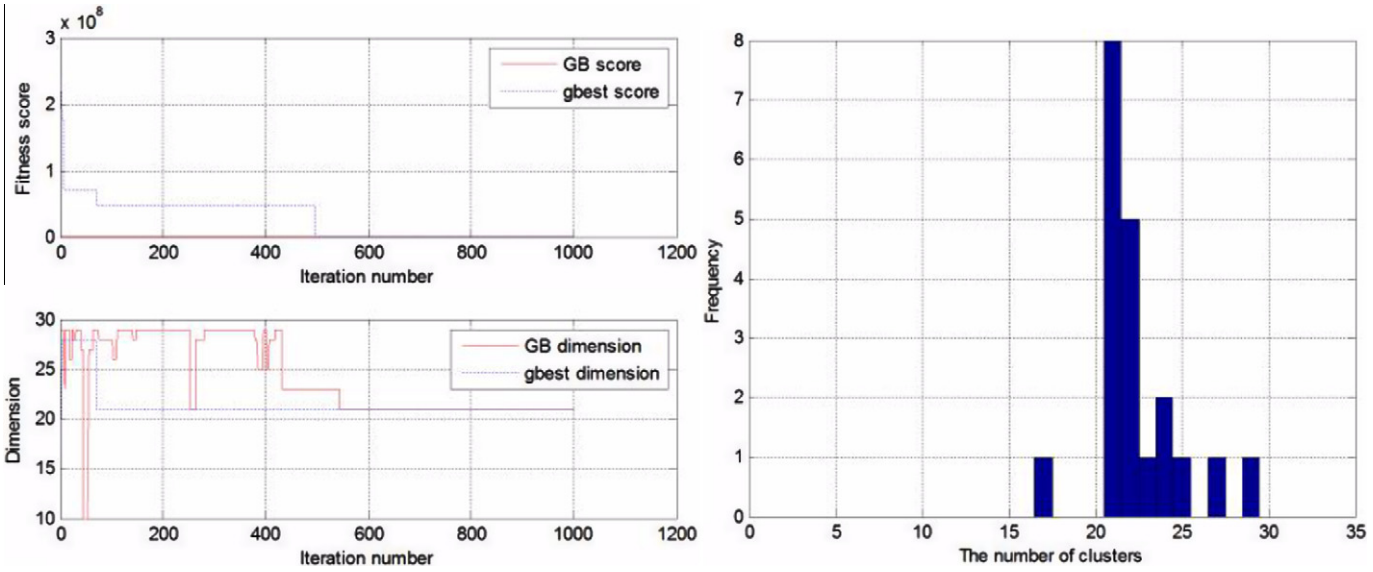

Fig. 5. Fitness score (left top) and dimension (left bottom) plots versus iteration number for a typical MD-PSO run. The resulting histogram plot (right) of cluster numbers which are determined by the proposed method.

Table 4
Overall performance comparison (in percent) for Flevoland dataset. The best performances are indicated in bold.

Method	Training area	Testing area
ECHO (Chen et al., 2007)	–	81.30
Wavelet-based (Fukuda & Hirosawa, 1999)	–	88.28
RBF-BP	95.50	92.05
NN (Zhang et al., 2009)	**98.62**	92.87
RBF-PSO	95.55	**93.36**

Next, the proposed evolutionary RBF classifier with the suggested feature set has been applied to the polarimetric image of the Flevoland site, an agricultural area (consists of primarily crop fields and forested areas) in The Netherlands. This original four-look fully polarimetric SAR data has a dimension of 750×1024 pixels with 11 identified crop classes {stem beans, potatoes, lucerne, wheat, peas, sugar beet, rape seed, grass, forest, bare soil, and water}. The available ground truth for eleven classes can be found in Ainsworth, Kelly, and Lee (2009). To compare classification results the same eleven training and testing sets are used with those of the NN-based (Zhang et al., 2009), wavelet-based (Fukuda & Hirosawa, 1999), and ECHO (Chen, Li, Pang, & Tian, 2007) classifiers. In Table 4, the overall accuracies in training and testing areas of the Flevoland dataset for the proposed RBF classifier trained using the BP and MD-PSO algorithms and three state of the art methods, the ECHO (Chen et al., 2007), wavelet-based (Fukuda & Hirosawa, 1999), and NN-based (Zhang et al., 2009) classifiers, are shown. The overall classification accuracies of the proposed RBF-based classifier framework are quite high. The percentage of correctly classified training and testing pixels in the Flevoland L-band image for the proposed evolutionary (MD-PSO) RBF method are given in Table 5. Fig. 6 shows the classification results of the proposed evolutionary RBF classifier for the Flevoland image.

The computational complexity of the proposed method depends on the following distinct processes: the pre-processing stage, feature extraction, post-processing, and RBF network classifier with MD-PSO dynamic clustering based training. Computation times of the first three stages are deterministic while a precise computational complexity analysis for the RBF training stage is not feasible as the proposed dynamic clustering technique based on PSO is in stochastic nature. All experiments in this section are performed on a computer with P-IV 2.4 GHz CPU and 1 GB RAM. Based on our experiments, for the data of San Francisco Bay area with a dimension of 900×1024 data points ($D = 921{,}600$), it takes 30 min to perform feature extraction and necessary pre- and post-processing stages. Most of this time is used to compute the GLCM and four texture features calculated from it. For computational complexity of RBF classifier training using MD-PSO process, there are certain attributes which directly affect the complexity

Table 5
Summary table of pixel-by-pixel classification results (in percent) of the proposed RBF-MDPSO method for the training and testing data of Flevoland.

	Training (Testing) data										
	Water	Forest	Stem beans	Potatoes	Lucerne	Wheat	Peas	Sugar beet	Bare soil	Grass	Rape seed
Water	99(98)	0(0)	0(0)	0(0)	0(0)	0(0)	0(0)	0(0)	0(0)	0(0)	1(2)
Forest	0(0)	95(97)	0(0)	0(0)	1(0)	0(0)	1(0)	1(0)	0(0)	2(3)	0(0)
Stem beans	0(0)	0(0)	95(97)	0(0)	5(2)	0(1)	0(0)	0(0)	0(0)	0(0)	0(0)
Potatoes	0(0)	0(0)	0(0)	99(96)	0(0)	0(0)	0(0)	1(4)	0(0)	0(0)	0(0)
Lucerne	0(0)	0(0)	2(2)	0(0)	98(97)	0(0)	0(0)	0(0)	0(0)	0(1)	0(0)
Wheat	0(0)	0(0)	0(0)	0(0)	2(4)	91(86)	4(4)	1(3)	0(0)	2(3)	0(0)
Peas	0(0)	0(0)	0(0)	0(0)	0(0)	1(0)	94(88)	2(7)	0(0)	0(0)	3(5)
Sugar beet	0(0)	0(0)	0(0)	0(0)	0(0)	0(2)	0(1)	95(91)	0(0)	4(5)	1(1)
Bare soil	0(0)	0(0)	0(0)	0(0)	0(0)	0(2)	0(0)	0(0)	99(97)	0(0)	1(1)
Grass	0(0)	0(0)	0(0)	0(0)	1(0)	0(1)	0(0)	2(4)	0(0)	97(95)	0(0)
Rape seed	2(2)	0(0)	0(0)	0(0)	0(0)	2(2)	1(2)	3(2)	3(7)	0(0)	89(85)

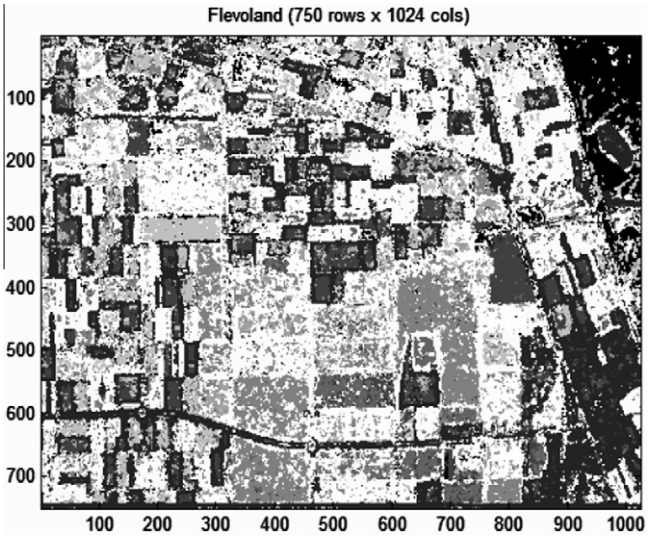

Fig. 6. The classification results of the proposed RBF-MDPSO technique on the L-band AIRSAR data over Flevoland.

such as swarm size (S), the number of iteration (*IterNo*) to terminate the MD PSO process, and the dimensions of data space (D). While the problem determines D, the computational complexity can still be controlled by S and *IterNo* settings. The further details of computational complexity analysis for the dynamic clustering technique based on MD-PSO can be found in Kiranyaz et al. (2010). For the same dataset, the average (over 10 runs) processing time to perform evolutionary RBF classifier training is found to be 30 min.

6. Conclusion

This paper presents a new polarimetric SAR image classification framework which is based on an efficient formation of covariance matrix elements, H/α/A decomposition with the backscattered power (span) information, and GLCM based texture features, and the RBF network classifier. Two different learning algorithms, the classical backpropagation and multidimensional particle swarm optimization, were applied for the proposed classifier training. In addition to determining the correct network parameters, the latter evolutionary technique (MD-PSO) also finds the best RBF network architecture (optimum number of Gaussian neurons and their centroids) within an architecture space and for a given input data space. The overall classification accuracies and qualitative classification maps for the San Francisco Bay and Flevoland datasets demonstrate the effectiveness of the proposed classification framework using an evolutionary RBF network classifier. Based on the experimental results using real polarimetric SAR data, the proposed method performs well compared to several state-of-the-art classifiers, however, more experiments using large volume of available data should be done for a general conclusion. The proposed technique employs evolutionary MD-PSO process for simultaneous training and evolution of RBF networks to achieve more accurate, robust, and automatic classification of polarimetric SAR images.

References

Ainsworth, T. L., Kelly, J. P., & Lee, J.-S. (2009). Classification comparisons between dual-pol, compact polarimetric and quad-pol SAR imagery. *ISPRS Journal of Photogrammetry and Remote Sensing, 64*, 464–471.

Chauvin, Y., & Rumelhart, D. E. (1995). *Back propagation: theory, architectures, and applications*. UK: Lawrence Erlbaum Associates Publishers.

Chen, E., Li, Z., Pang, Y., & Tian, X. (2007). Quantitative evaluation of polarimetric classification for agricultural crop mapping. *Photogrammetric Engineering and Remote Sensing, 73*(3), 279–284.

Clausi, D. A. (2002). An analysis of co-occurrence texture statistics as a function of grey level quantization. *Canadian Journal of Remote Sensing, 28*(1), 45–62.

Clausi, D. A., & Yue, B. (2004). Comparing co-occurrence probabilities and Markov random fields for texture analysis of SAR sea ice imagery. *IEEE Transactions on Geoscience and Remote Sensing, 42*(1), 215–228.

Cloude, S. R., & Pottier, E. (1996). A review of target decomposition theorems in radar polarimetry. *IEEE Transactions on Geoscience and Remote Sensing, 34*(2), 498–518.

Cloude, S. R., & Pottier, E. (1997). An entropy based classification scheme for land applications of polarimetric SAR. *IEEE Transactions on Geoscience and Remote Sensing, 35*, 68–78.

Ersahin, K., Scheuchl, B., & Cumming, I. (2004). Incorporating texture information into polarimetric radar classification using neural networks. In *Proceedings of the IEEE International Geoscience and Remote Sensing Symposium, Anchorage, USA, September* (Vol. 1, pp. 560–563).

Fang, C., Wen, H., & Yirong, W. (2006). An improved Cloude–Pottier decomposition using H/α/span and complex Wishart classifier for polarimetric SAR classification. In *Proceedings of the CIE October* (pp. 1–4).

Ferro-Famil, L., Pottier, E., & Lee, J. S. (2001). Unsupervised classification of multifrequency and fully polarimetric SAR images based on the H/A/Alpha-Wishart classifier. *IEEE Transactions on Geoscience and Remote Sensing, 39*(11), 2332–2342.

Fukuda, S., & Hirosawa, H. (1999). A wavelet-based texture feature set applied to classification of multifrequency polarimetric SAR images. *IEEE Transactions on Geoscience and Remote Sensing, 37*(5), 2282–2286.

US Geological Survey Images. <http://www.terraserver-usa.com>.

Haykin, S. (1998). *Neural networks: A comprehensive foundation*. USA: Prentice hall.

Ince, T. (2010). Polarimetric SAR image classification using a radial basis function neural network. In *Proceedings of The Progress in Electromagnetics Research Symposium (PIERS 2010), Cambridge, USA, July*.

Ince, T. (2010). Unsupervised classification of polarimetric SAR image with dynamic clustering: An image processing approach. *Advances in Engineering Software, 41*(4), 636–646.

Khan, K. U., Yang, J., & Zhang, W. (2007). Unsupervised classification of polarimetric SAR images by EM algorithm. *IEICE Transactions on Communications, 90*(12), 3632–3642.

Kiranyaz, S., Ince, T., Yildirim, A., & Gabbouj, M. (2009). Evolutionary artificial neural networks by multi-dimensional particle swarm optimization. *Neural Networks, 22*(10), 1448–1462.

Kiranyaz, S., Ince, T., Yildirim, A., & Gabbouj, M. (2010). Fractional particle swarm optimization in multi-dimensional search space. *IEEE Transactions on Systems, Man, and Cybernetics – Part B, 40*(2), 298–319.

Kong, J. A., Swartz, A. A., Yueh, H. A., Novak, L. M., & Shin, R. T. (1988). "Identification of terrain cover using the optimum polarimetric classifier. *Journal of Electromagnetic Waves and Applications, 2*(2), 171–194.

Lee, J. S., Grunes, M. R., Ainsworth, T., Du, L.-J., Schuler, D., & Cloude, S. R. (1999). Unsupervised classification using polarimetric decomposition and the complex Wishart classifier. *IEEE Transactions on Geoscience and Remote Sensing, 37*(5), 2249–2257.

Lee, J. S., Grunes, M. R., & de Grandi, G. (1999). Polarimetric SAR speckle filtering and its implications for classification. *IEEE Transactions on Geoscience and Remote Sensing, 37*(5), 2363–2373.

Lee, J. S., Grunes, M. R., & Kwok, R. (1994). Classification of multi-look polarimetric SAR imagery based on complex Wishart distribution. *International Journal of Remote Sensing, 15*(11), 2299–2311.

Pittner, S., & Kamarthi, S. V. (1999). Feature extraction from wavelet coefficients for pattern recognition tasks. *IEEE Transactions on Pattern Analysis and Machine Intelligence, 21*, 83–88.

Poggio, T., & Girosi, F. (1989). A theory of networks for approximation and learning, A.I. Memo No. 1140, M.I.T. A.I Lab.

The Polarimetric SAR Data Processing and Educational Tool (PolSARPro). <http://www.earth.esa.int/polsarpro/datasets.html>.

Pottier, E., & Lee, J. S. (2000). Unsupervised classification scheme of POLSAR images based on the complex Wishart distribution and the H/A/alpha-polarimetric decomposition theorem. In *Proceedings of the 3rd EUSAR 2000 Conference May*.

Riedmiller, M., & Braun, H. (1993). A direct adaptive method for faster backpropagation learning: The RPROP algorithm. In *Proceedings of the IEEE international conference on neural networks* (pp. 586–591).

Shi, Y., & Eberhart, R. C. (1998). A modified particle swarm optimizer. In *Proceedings of the IEEE Congress on Evolutionary Computation* (pp. 69–73).

Tan, C. P., Lim, K. S., Ewe, H. T. (2007). Image processing in polarimetric SAR images using a hybrid entropy decomposition and maximum likelihood (EDML). In *Proceedings of the International Symposium on Image and Signal Processing and Analysis (ISPA), September* (pp. 418–422).

Tran, T. N., Wehrens, R., Hoekman, D. H., & Buydens, L. M. C. (2005). Initialization of Markov random field clustering of large remote sensing images. *IEEE Transactions on Geoscience and Remote Sensing, 43*(8), 1912–1919.

van Zyl, J. J. (1989). Unsupervised classification of scattering mechanisms using radar polarimetry data. *IEEE Transactions on Geoscience and Remote Sensing, 27*, 36–45.

Wu, Y., Ji, K., Yu, W., & Su, Y. (2008). Region-based classification of polarimetric SAR images using Wishart MRF. *IEEE Geoscience and Remote Sensing Letters, 5*(4), 668–672.

Yang, S. Y., Wang, M., & Jiao, L. C. (2009). Radar target recognition using contourlet packet transform and neural network approach. *Signal Processing, 89*(4), 394–409.

Ye, Zhen, Lu, Cheng-Chang (2002). Wavelet-based unsupervised SAR image segmentation using hidden markov tree models. In *Proceedings of the16th international conference on pattern recognition (ICPR'02)* (Vol. 2, p. 20729).

Zhang, Y. D., Wu, L.-N., & Wei, G. (2009). A new classifier for polarimetric SAR images. *Progress in Electromagnetics Research, PIER, 94*, 83–104.

Zhang, L., Zou, B., Zhang, J., & Zhang, Y. (2010). Classification of polarimetric SAR image based on support vector machine using multiple-component scattering model and texture features. *EURASIP Journal on Advances in Signal Processing*. doi:10.1155/2010/960831.